RSC Advances

ROYAL SOCIETY OF CHEMISTRY

www.rsc.org/advances

RSC Advances

ARTICLE

Construction and coulodynamic characterization of PPy-DBS-MWCNT/tape bilayer artificial muscles

Received 00th January 20xx,
Accepted 00th January 20xx

DOI: 10.1039/x0xx00000x

www.rsc.org/

Toribio F. Otero[a], Johanna Schumacher[b*] and Victor H. Pascual[a]

Polypyrrole-dodecylbenzenesulphonate-multi-walled carbon nanotube (PPy-DBS-MWCNT) films, thick enough (48.6 μm) to be peeled off from the steel electrode, were electrogenerated. Bilayer PPy-DBS-MWCNT/tape artificial muscles were constructed and submitted to potential sweeps with parallel video-recording of their angular displacements. The coulodynamic (angle-charge) responses reveal that the composite shrinks/swells by oxidation/reduction, respectively, due to the reaction-driven cation exchange. Reversible bending movements of 106° occur under faradaic (linear) control of the consumed charge. Minor deviations and hysteresis were identified with irreversible reactions and osmotic processes. The muscle is a faradaic motor.

1 Introduction

Artificial muscles are polymeric motors transducing electrical energy into mechanical energy through reversible volume variations of the muscle material driven by electrochemical reactions.[1–6] During the oxidation/reduction of the electroactive material counterions and solvent molecules are exchanged with the electrolyte to keep the charge balance inside the film and the osmotic balance between the material and the electrolyte.[7–9] Reversible electrochemical reactions drive the reversible generation/destruction of free volume required to lodge/expel those molecules and ions. Bending bilayer artificial muscles transduce minor reaction-driven ionic exchanges into large angular (> 30°) displacements.[10–15] They are electro-chemo-mechanical transducers.

Electroactive films of different materials are being used to develop artificial muscles: conducting polymers[16–29], carbon based materials such as carbon nanotubes (CNT)[30–37] and so on. With the aim of enhanced actuation performance efforts have been made to combine conducting polymers and carbon nanotubes and to study their applicability in artificial muscles.[38,39] Different fabrication methodologies have been developed to produce artificial muscles based on those composites. In early approaches polyaniline solution was coated on CNT sheets[39] or polyaniline-CNT solution on electrogenerated PPy fibers[40] and dried on a hot plate. In addition, other coating techniques of CNT sheets were investigated such as electrogeneration of PPy[38,41] and vapor depositioning of the monomer.[38] Using one of those coating techniques multilayer artificial muscles were fabricated of laminates of CNT sheets and electrogenerated polypyrrole (PPy) layers at constant current.[42] The fabrication process requires iterative steps comprising initial PPy depositioning on a glassy carbon plate, placement of the CNT sheets, densification with ethanol and so on. Finally, the laminate actuator is peeled off the electrode. Other laminated artificial muscles were produced using a flexible polymer layer spin-coated with solutions of CNT or CNT-PEDOT on which a PPy-DBS coating was electrogenerated.[43] Another method was developed to obtain full-polymeric composite trilayer artificial muscles in which the electroactive films are casted from a mixture of CNT, ionic liquid, base polymer and polyaniline particles combined under heat pressing.[44] Furthermore, wet spinning techniques were utilized to fabricate polyaniline-CNT fibers from solutions[45] and to coat a polyaniline-CNT layer on cellular paper.[46]

The investigation of the actuation performance of those actuators showed promising results. Voltammetric responses revealed the electroactivity of the composite artificial muscles [42,43,45], greater current flow, hence higher reduction and oxidation charges, and more distinct reduction and oxidation peaks in comparison with neat conducting polymer.[42,45] The resulting bending displacements showed enhanced actuation[42] although higher displacements were observed for lower CNTs amounts in a trilayer artificial muscle.[43] CNTs influence the range of movement.[40] In addition, isotonic actuation experiments revealed improved performance under load with the presence of CNTs and reduction in material creeping.[40,42,45] Long-term cycling stability test showed up to 14,000 cycles at 1 Hz (square potential waves).[43]

Despite those promising properties, the previous reported fabrication processes are complex. The generation of composite monolayers would enable the construction of bending bilayer artificial muscles. Thin films of the composite

[a] Laboratory of Electrochemistry and Intelligent Materials. Technical University of Cartagena. ETSII. Campus Alfonso XIII, 30203, Cartagena, Spain. E-mail: toribio.fotero@upct.es
[b] Arquimea Ingeniería, Margarita Salas 10, 28919, Leganés, Spain. E-mail: jschumacher@arquimea.com

of polypyrrole, carbon nanotubes and dodecylbenzene sulphonate, required to prepare a stable suspension, PPy-DBS-MWCNT, have been electrogenerated from one solution before on metal electrodes or other substrates.[47–50] Those thin films cannot be peeled off from the electrode or used for the construction of artificial muscles. Here we present the electrosynthesis of PPy-DBS-MWCNT films, which are thick enough to be removed from the electrode to get self-supported films. Those films will be used for the construction and subsequent characterization of bilayer PPy-DBS-MWCNT/tape artificial muscles. Electrochemical and electrodynamical characterization will be used for the investigation of the reaction kinetics driving the artificial muscle and the actuation performance.

2 Experimental

2.1 Materials

Pyrrole (Fluka) was distilled using a diaphragm vacuum pump and stored at − 10° C. Multi-walled carbon nanotubes (MWCNT) (Sigma-Aldrich, purity >90%, outer diameter 10-15 nm, inner diameter 2-6 nm, length 0.1–10 μm), sodium perchlorate ($NaClO_4$) (Sigma-Aldrich) and sodium dodecylbenzenesulfonate (NaDBS) (Sigma-Aldrich) were used as received. All aqueous solutions were prepared with ultrapure water from Millipore Milli-Q equipment.

2.2 Equipment and Experimental Conditions

The electrochemical studies were performed using an Autolab potentiostat/galvanostat PGSTAT302 controlled by NOVA 1.11 software and a three electrode one-compartment electrochemical cell. An Ag/AgCl (3 M KCl) electrode from Metrohm was used as reference electrode (RE) and stainless steel plates as counter electrode (CE). The electrochemical characterization was performed in 0.1 M $NaClO_4$ aqueous solutions. The total mass of the electropolymerized films was determined with a Sartorius SC2 balance (±0.1 mg) from the mass difference between coated and uncoated electrode. The thickness of the electrogenerated films (peeled off from the electrode) was determined using a Helios Preisser digital micrometer (±1 μm). The angular displacements of the bilayer muscle were video-recorded using a 1080p high-resolution camera and measured from the video-frames using a Matlab program. Energy-dispersive X-ray (EDX) analysis was obtained with a Hitachi TM-3000 SEM with an Oxford Instrument SwiftED 3000 EDX analyzer.

2.3 Film Preparation

The PPy-DBS-MWCNT film was electrochemically synthesized at room temperature from 0.1 wt% MWCNT, 0.03 M NaDBS and 0.1 M PPy aqueous solution. The MWCNT were dispersed in 0.03 M NaDBS aqueous solution in an ultrasonic bath for 1 h. Afterwards the monomer was added and the monomeric solution was prepared using the magnetic stirrer for 30 min at 60 rpm. The working electrode (WE) was a stainless steel electrode (900 mm²) placed symmetrically between two parallel CEs (total area 1800 mm²), at a distance of 1 cm. In this way a uniform electric field allowed the electropolymerization by potential step from -0.2 V for 1s to 0.8 V for 3600s of two uniform films, one on each side of the WE. The influence of the synthesis conditions and the electrochemical characterization (voltammetric, coulovoltammetric and chronoamperometric) of the self-supported film electrodes under different experimental conditions were described in a separate manuscript.[51]

3 Results and Discussion

3.1 PPy-DBS-MWCNT/tape bilayer artificial muscles

Two (one per WE side, Figure 1a1) thick films (20 mm x 10 mm x 48.6 μm) were rinsed and kept in ultrapure water over night to eliminate adsorbed DBS (it causes adhesion problems or muscle delamination during electrochemical actuation). Then the coated electrode was dried in air for one day and removed from the electrode (Figure 1a2). Each removed composite film was weighed; the film thickness (48.6 μm) was determined and attached to a non-conductive double-sided tape (Figure 1a3) applying some pressure with a cylindrical rod for good adherence. The tape was adhered to the composite film on the composite/electrolyte side during the electropolymerization process. Longitudinal strips (20 mm x 3 mm) were cut (Figure1a4) from the PPy-DBS-MWCNT/tape bilayer. A transversal narrow (1 mm) paint strip was painted on the PPy-DBS-MWCNT layer at 15 mm from the bottom and 5 mm from the top (Figure1c). The electrical contact was connected at the top. The muscle was immersed with the electrolyte vortex below the transversal paint strip. The paint strip closes the composite pores avoiding the electrolyte ascension by capillarity towards the metallic clamp and the concomitant electrolyte reactions during the electrochemical characterization of the muscle. In addition, the paint strip acts as a mark for the immersion: the electrolyte meniscus must be below the paint strip ensuring a constant immersed PPy-DBS-MWCNT surface area of 45 mm² with a corresponding mass of 2.1 mg: this is the electroactive mass which electrochemical reactions will drive the muscle actuation. Figure1b shows the final bilayer muscle ready to be used as WE (Figure2a) for the electro-chemo-dynamical characterization.

3.2 Electro-chemo-dynamical characterization

The bilayer muscle was submitted to consecutive potential sweeps between –1200 mV and 700 mV at 6 mVs^{-1} until stationary voltammetric responses (Figure 3, after two cycles). The angular displacement followed by the muscles was video recorded in parallel. The angular position corresponding to each potential was determined (Figure 2b) from the concomitant video-frame. The PPy-DBS-MWCNT layer (electroactive) was located on the left side of the bilayer and the tape (passive) on the right side (Figures 1c and 2a). Figure 4 shows, overlapped, the coulovoltammetric (charge-potential, Q-E) and the dynamovoltammetric (angle-potential, α-E) responses. Pictures from Figure 6 show the evolution of the

bilayer position during one of the consecutive potential cycles: point 1 to 10 are the same on Figures 3 and 4, correlating to pictures 1 to 10. Clockwise bending indicates the reaction driven shrinking of the electroactive PPy-DBS-MWCNT layer; anticlockwise bending movements indicates the reaction-driven swelling of the composite. Angular movements observed during the potential cycle will be used as a tool to clarify the reactions originating the volumetric changes and bending movements.

3.3 Coulovoltammetric (Q-E) and dynamo-voltammetric (α-E) response

The coulovoltammetric (Q-E) response (Figure 4 red line) from the muscle is obtained by integration of the voltammetric response (Figure 3) using the sweep rate (6 mVs^{-1}) as conversion factor from potential to time. Positive charge increments mean charge consumed by oxidation of the composite layer and negative charge increments quantify the composite reduction charge. The dynamo-voltammetric (α-E) response is depicted by Figure 4 (green line), with a total bending displacement, under those experimental conditions, of 106° (Figure 6, pictures 2 to 6).

The film oxidation is initiated after point 2 (Q-E minimum, red line). The highest oxidized state under those experimental conditions is attained at point 6 where the Q-E maximum is reached (Figure 4 red line) by consumption of a specific charge of 96.05 mC mg^{-1}. As expected for a faradaic device (the specific charge controls the number of exchanged ions and solvent molecules, the concomitant volume variation to lodge/expel those ions and the subsequent angular displacement promoted by the volumetric change) the muscle bottom describes a clockwise angular displacement during the material oxidation from point 2 to 6 (Figure 4 green line and 6). The maximum angular displacement corresponds to the maximum oxidation charge at point 6.

Reduction occurs at the beginning of each cycle from point 1 to 2 defining the Q-E minimum and from point 6 to 10 (Figure 4 red line). Anticlockwise angular displacements are observed between point 1 and 2 and from point 6 to 10 (Figure 4, green line and Figure 6, pictures 1 to 2 and 6 to 10).

At the end of the potential cycle (point 10) neither the initial angular position nor the initial charge are recovered (Figure 4). The Q-E response includes two parts: a closed loop on the right side and an open part on the left side. The closed loop defines the specific charge (96.5 mC mg^{-1}) required for the reversible reactions of the electroactive composite film: specific oxidation charges equal specific reduction charges. The open part, from 1 to 2, is a reduction irreversible specific charge not recovered during the cycle. An irreversible specific charge (Q_{irr} in Figure 4) of 6.89 mC mg^{-1} (7.2 % of the reversible charge) is missed. It was attributed to the presence of irreversible hydrogen evolution from the DBS component of the composite.[12]

The dynamo-voltammetric (α-E) response follows an almost parallel evolution to that described by the Q-E response but now the cycle remains open, not recovering the initial position. The final position is shifted (Δα) about 5° clockwise (4.7 % of the total bending displacement) related to the initial position. This angular displacement by cycle is known as creeping effect and has been attributed to the irreversible reduction reactions at higher cathodic potentials than -1100 mV: chemical creeping.[12] Both, presence of irreversible reactions and parallel chemical creeping promotes the progressive clockwise shift of the angular displacement for consecutive cycles and a slow chemical degradation of the film electroactivity (redox charge) per cycle. The presence of chemical creeping originates a low control of the muscle position on consecutive cycles. The consumption of irreversible charges and polymeric degradation decrease the muscle efficiency and the muscle lifetime.

3.4 Coulodynamic (α-Q) Response

For the examination of the faradaic nature of the device the experimental results are represented as coulodynamic (angle-charge, α-Q) response: angular displacement of the muscle (α) as a function of the consumed anodic or cathodic charge (Q) (Figure 5). Positive/negative charge increments mean oxidation/reduction reactions, respectively. Positive/negative angular increments on Figure 5 mean clockwise/anticlockwise angular displacements and reaction-driven shrinking/swelling of the PPy-DBS-MWCNT layer, respectively.

The coulodynamic response shows (point 1 to point 2) the consumption of low reduction charges originating anticlockwise bending giving a hook shape that correlates with the initial reduction-swelling of the composite film (Figure 6, picture 1 and 2). From point 2 to 6 the flow of oxidation charges drives clockwise bending displacements forced by the PPy-DBS-MWCNT film shrinking until the maximum angular displacement that corresponds to the maximum oxidation charge (Figure 5). At point 6 the film reduction starts going on until point 10, giving anticlockwise bending displacements due to the reaction-driven swelling of the PPy-DBS-MWCNT film.

For the same charge the muscle presents a different angular position during the oxidation and the reduction branch: this is a dynamical hysteresis effect. The maximal dynamic hysteresis is 16.77° at 31.2 mC mg^{-1}. Similar dynamical hysteresis observed with a PPy-DBS bending artificial muscle was related to osmotic and electroosmotic physical processes driving the exchange of solvent that follow the ionic exchanges.[11] At the end of the cycle the muscle does not recover the initial position (chemical creeping effect) and some irreversible charge was consumed by irreversible reactions. The coulodynamic response reveal both, the creeping effect (Figure 4, dynamovoltammetric response) and the irreversible charge (Figure 4, coulovoltammetric response).

In average, the coulodynamic response depicts distinctly two linear sections. Below 31.2 mC mg^{-1} the linear relationship is:

$$\alpha = 1.52° \, mC^{-1} \, mg \cdot Q + 48.03° \quad (1)$$

with the slope k'=1.52° mC^{-1} mg and correlation coefficient r^2 = 0.75

And above 31.2 mC mg^{-1} the linear relationship is:

$\alpha = 0.68° \text{ mC}^{-1} \text{ mg} \cdot Q + 70.15°$ (2)

with the slope k'= 0.68° mC^{-1} mg and correlation coefficient r^2 = 0.78

The slope of the faradaic relationship has been defined as the coulodynamic constant of the system (electroactive material, tape, electrolyte): angular displacement (°) described by unit of consumed specific charge (mC mg^{-1}).[2] The low correlation coefficients are here related to the dynamic hysteresis and the initial hook shape displacement. Small deviations from the linear dependence of the angular displacement from the involved charge were attributed to the osmotic exchange of water: a physical process that follows the electrochemical reactions. The presence of two linear relationships can be attributed to the fact that the two electroactive components of the composite film, PPy and MWCNT, follow redox processes in aqueous solution with predominant exchange of cations.[52–56] The experimental result should support the presence of the two concomitant reactions occurring in different potential domains:

$$PPy^*CNT^*(DBS^-Na^+)_n \leftrightharpoons PPy^*CNT^{n+}(DBS^-)_n + n(Na^+) + ne^- \quad (3)$$
$$PPy^*CNT^*(DBS^-Na^+)_n \leftrightharpoons PPy^{n+}CNT^*(DBS^-)_n + n(Na^+) + ne^- \quad (4)$$

In both reactions, PPy* and CNT* are the active centers in the film that store positive charge after oxidation, DBS^- represents the anion trapped in the film during the electrogeneration, Na^+ is the cation penetrating during the reduction to compensate the charge of the macroions DBS^-. Reaction 3 should prevail at high anodic potentials and reaction 4 occurs at more cathodic potentials: the different kinetics originate two coulodynamic slopes (Figure 5).

3.5 EDX analysis of the oxidized and reduced films

The energy-dispersive X-ray (EDX) spectra depict (Figure 7) for the oxidized and reduced film a clear sodium (Na) signal at 1.05 keV and a minor chloride (Cl) signal at 2.03 keV. The reduced film presents a high Na content, which decreases significantly in the oxidized state. The Cl content is very low in both states being a little bit higher in the oxidized state. As the electrolyte was 0.1 M $NaClO_4$ aqueous solution, this fact points to dominant Na^+ incorporation during reduction and expulsion during oxidation. The EDX analysis corroborates the reaction-driven exchange of cations. Reactions 3 and 4 drive the swelling of the composite layer by electrochemical reduction and its shrinking under oxidation, as indicated by the experimental results described in section 3.4 for the coulodynamic (α-Q) response.

4 Conclusion

The generation of thick PPy-DBS-MWCNT allows the construction of bilayer bending artificial muscles. Under voltammetric control the bilayer describes a reversible angular displacement of 106° consuming a reversible specific charge of 96.05 mC mg^{-1}. The sense of the angular displacements indicates the entrance of cations during the electrochemical reduction of the composite layer and their expulsion during oxidation. Those ionic exchanges are corroborated by EDX analysis. The coulodynamic response corroborates the faradaic nature of the device (charge controls angular displacement) with two slopes related to the reaction kinetics of the two electroactive components. PPy-DBS-MWCNT/tape bilayer muscles are faradaic motors. Some irreversible charge is consumed per cycle originating creeping effects and polymeric degradation and concomitant decrease of the position control and lifetime.

Acknowledgement

This project has received funding from the European Union's Horizon 2020 research and innovation program under the Marie Sklodowska-Curie grant agreement No 641822.

Notes and references

1 T. F. Otero, *Conducting Polymers*, The Royal Society of Chemistry, 2016.
2 T. F. Otero, J. G. Martinez and J. Arias-Pardilla, *Electrochimica Acta*, 2012, **84**, 112–128.
3 Y. Bar-Cohen, *Electroactive Polymer (EAP) Actuators as Artificial Muscles: Reality, Potential, and Challenges*, Society of Photo Optical, 2004.
4 T. Mirfakhrai, J. D. Madden and R. H. Baughman, *Mater. Today*, 2007, **10**, 30–38.
5 K. Asaka and H. Okuzaki, *Soft Actuators: Materials, Modeling, Applications, and Future Perspectives*, Springer, 2014.
6 E. Smela, *Adv. Mater.*, 2003, **15**, 481–494.
7 L. Bay, T. Jacobsen, S. Skaarup and K. West, *J. Phys. Chem. B*, 2001, **105**, 8492–8497.
8 T. F. Otero and J. G. Martinez, *Chem. Mater.*, 2012, **24**, 4093–4099.
9 T. F. Otero, *Polym. Rev.*, 2013, **53**, 311–351.
10 T. F. Otero and M. T. Cortes, *Chem. Commun.*, 2004, 284–285.
11 M. Fuchiwaki, J. G. Martinez and T. F. Otero, *Electrochimica Acta*, 2016, **195**, 9–18.
12 L. Valero, J. G. Martinez and T. F. Otero, *J. Solid State Electrochem.*, 2015, **19**, 2683–2689.
13 M. Fuchiwaki, J. G. Martinez and T. F. Otero, *Adv. Funct. Mater.*, 2015, **25**, 1535–1541.
14 M. Fuchiwaki and T. F. Otero, *J. Mater. Chem. B*, 2014, **2**, 1954–1965.
15 T. F. Otero and J. G. Martinez, *Sens. Actuators B Chem.*, 2014, **199**, 27–30.
16 N. Aydemir, P. A. Kilmartin, J. Travas-Sejdic, A. Kesküla, A.-L. Peikolainen, J. Parcell, M. Harjo, A. Aabloo and R. Kiefer, *Sens. Actuators B Chem.*, 2015, **216**, 24–32.
17 T. F. Otero and J. M. Sansinena, *Bioelectrochem. Bioenerg.*, 1995, **38**, 411–414.
18 K. Kaneto, M. Kaneko, Y. Min and A. G. MacDiarmid, *Synth. Met.*, 1995, **71**, 2211–2212.
19 A. D. Santa, D. D. Rossi and A. Mazzoldi, *Synth. Met.*, 1997, **90**, 93–100.
20 A. Hutchison, T. Lewis, S. Moulton, G. Spinks and G. Wallace, *Synth. Met.*, 2000, **113**, 121–127.
21 E. W. Jager, E. Smela and O. Inganäs, *Science*, 2000, **290**, 1540–1545.

22 G. Alici and N. N. Huynh, *Sens. Actuators Phys.*, 2006, **132**, 616–625.
23 F. Vidal, C. Plesse, G. Palaprat, A. Kheddar, J. Citerin, D. Teyssié and C. Chevrot, *Synth. Met.*, 2006, **156**, 1299–1304.
24 R. Kiefer, S. Y. Chu, P. A. Kilmartin, G. A. Bowmaker, R. P. Cooney and J. Travas-Sejdic, *Electrochimica Acta*, 2007, **52**, 2386–2391.
25 K. Yamato and K. Kaneto, *Anal. Chim. Acta*, 2006, **568**, 133–137.
26 M. Fuchiwaki, K. Tanaka and K. Kaneto, *Sens. Actuators Phys.*, 2009, **150**, 272–276.
27 L. Bay, K. West, P. Sommer-Larsen, S. Skaarup and M. Benslimane, *Adv. Mater.*, 2003, **15**, 310–313.
28 Q. Pei and O. Inganäs, *J. Phys. Chem.*, 1992, **96**, 10507–10514.
29 R. H. Baughman, *Synth. Met.*, 1996, **78**, 339–353.
30 R. H. Baughman, C. Cui, A. A. Zakhidov, Z. Iqbal, J. N. Barisci, G. M. Spinks, G. G. Wallace, A. Mazzoldi, D. De Rossi and A. G. Rinzler, *Science*, 1999, **284**, 1340–1344.
31 J. Foroughi, G. M. Spinks, G. G. Wallace, J. Oh, M. E. Kozlov, S. Fang, T. Mirfakhrai, J. D. Madden, M. K. Shin and S. J. Kim, *Science*, 2011, **334**, 494–497.
32 J. Fraysse, A. Minett, O. Jaschinski, G. Duesberg and S. Roth, *Carbon*, 2002, **40**, 1735–1739.
33 B. J. Landi, R. P. Raffaelle, M. J. Heben, J. L. Alleman, W. VanDerveer and T. Gennett, *Nano Lett.*, 2002, **2**, 1329–1332.
34 S. Roth and R. H. Baughman, *Curr. Appl. Phys.*, 2002, **2**, 311–314.
35 U. Vohrer, I. Kolaric, M. Haque, S. Roth and U. Detlaff-Weglikowska, *Carbon*, 2004, **42**, 1159–1164.
36 T. Mirfakhrai, J. Oh, M. Kozlov, E. C. W. Fok, M. Zhang, S. Fang, R. H. Baughman and J. D. Madden, *Smart Mater. Struct.*, 2007, **16**, S243.
37 K. Asaka, K. Mukai, T. Sugino and K. Kiyohara, *Polym. Int.*, 2013, **62**, 1263–1270.
38 G. M. Spinks, G. G. Wallace, C. D. Carter, D. Zhou, L. S. Fifield, C. R. Kincaid and R. H. Baughman, in *SPIE's 8th Annual International Symposium on Smart Structures and Materials*, International Society for Optics and Photonics, 2001, pp. 199–208.
39 M. Tahhan, V.-T. Truong, G. M. Spinks and G. G. Wallace, *Smart Mater. Struct.*, 2003, **12**, 626.
40 G. M. Spinks, B. Xi, V.-T. Truong and G. G. Wallace, *Synth. Met.*, 2005, **151**, 85–91.
41 K. Yamato, K. Asaka, K. Hata and H. Oike, *Sens. Actuators B Chem.*, 2012, **161**, 1010–1017.
42 W. Zheng, J. M. Razal, P. G. Whitten, R. Ovalle-Robles, G. G. Wallace, R. H. Baughman and G. M. Spinks, *Adv. Mater.*, 2011, **23**, 2966–2970.
43 R. Kiefer, R. Temmer, T. Tamm, J. Travas-Sejdic, P. A. Kilmartin and A. Aabloo, *Synth. Met.*, 2013, **171**, 69–75.
44 T. Sugino, K. Kiyohara, I. Takeuchi, K. Mukai and K. Asaka, *Carbon*, 2011, **49**, 3560–3570.
45 V. Mottaghitalab, B. Xi, G. M. Spinks and G. G. Wallace, *Synth. Met.*, 2006, **156**, 796–803.
46 S. Yun and J. Kim, *J. Phys. Appl. Phys.*, 2006, **39**, 2580.
47 G. Z. Chen, M. S. Shaffer, D. Coleby, G. Dixon, W. Zhou, D. J. Fray and A. H. Windle, *Adv. Mater.*, 2000, **12**, 522–526.
48 J. Hernández-Ferrer, A. Ansón-Casaos and M. T. Martínez, *Electrochimica Acta*, 2012, **64**, 1–9.
49 Y. Lu, T. Li, X. Zhao, M. Li, Y. Cao, H. Yang and Y. Y. Duan, *Biomaterials*, 2010, **31**, 5169–5181.
50 C. Peng, J. Jin and G. Z. Chen, *Electrochimica Acta*, 2007, **53**, 525–537.
51 T. F. Otero and J. Schumacher, *J. Electroanal. Chem.*, Submitted.
52 J. N. Barisci, G. G. Wallace and R. H. Baughman, *J. Electroanal. Chem.*, 2000, **488**, 92–98.
53 J. N. Barisci, G. G. Wallace and R. H. Baughman, *J. Electrochem. Soc.*, 2000, **147**, 4580–4583.
54 J. G. Martinez and T. F. Otero, *J. Phys. Chem. B*, 2012, **116**, 9223–9230.
55 L. V. Conzuelo, J. Arias-Pardilla, J. V. Cauich-Rodríguez, M. A. Smit and T. F. Otero, *Sensors*, 2010, **10**, 2638–2674.
56 K. Mukai, K. Asaka, K. Hata, T. Fernández Otero and H. Oike, *Chem. Eur. J.*, 2011, **17**, 10965–10971.

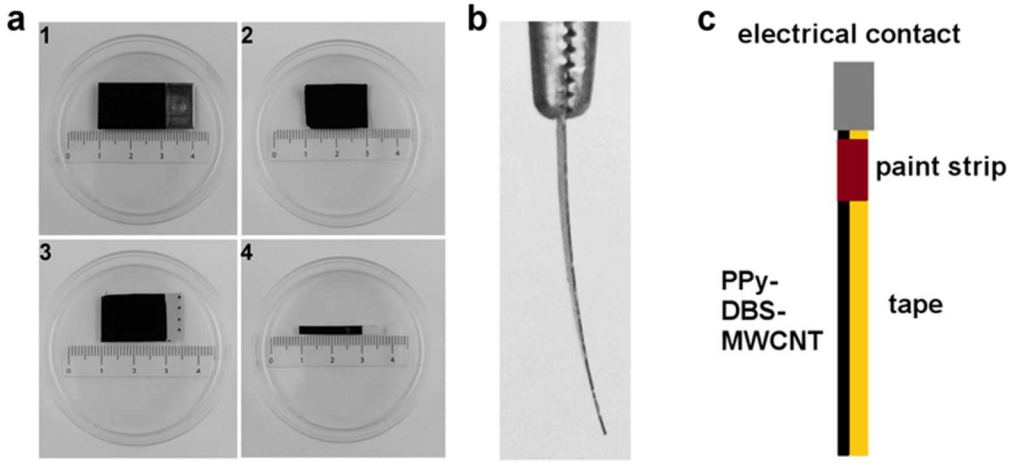

Figure 1 Construction of bilayer PPy-DBS-MWCNT/tape muscles: (a) (1) coated electrode (2) self-supported PPy-DBS-MWCNT film (3) PPy-DBS-MWCNT/tape bilayer with marks for several muscles (4) PPy-DBS-MWCNT/tape muscle (b) bilayer muscle lateral view with PPy-DBS-MWCNT on the left and the tape on the right (c) scheme of the bilayer muscle
65x30mm (300 x 300 DPI)

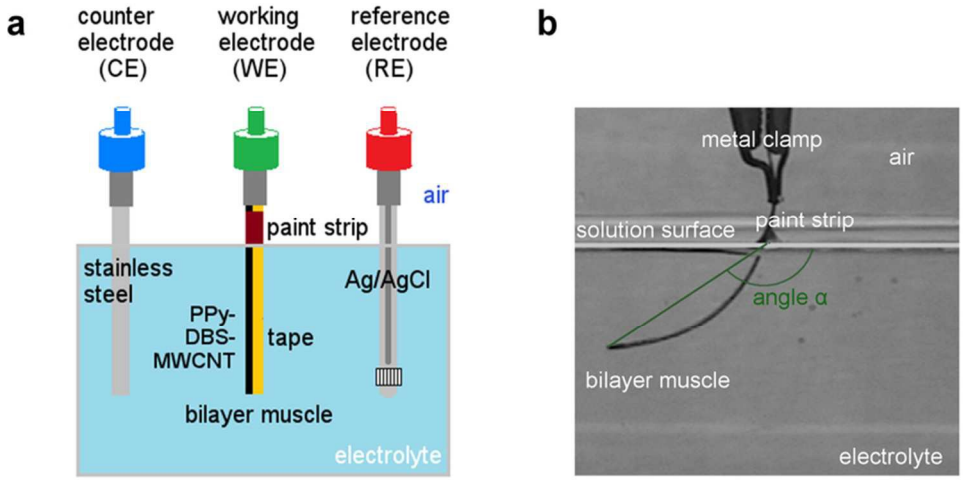

Figure 2 Experimental set-up for electro-chemo-dynamical characterization: (a) electrochemical cell with Ag/AgCl reference electrode, bilayer muscles as working electrode and stainless steel counter electrode (b) PPy-DBS-MWCNT/tape bilayer muscle in the electrolyte with indication of the angular position
75x40mm (300 x 300 DPI)

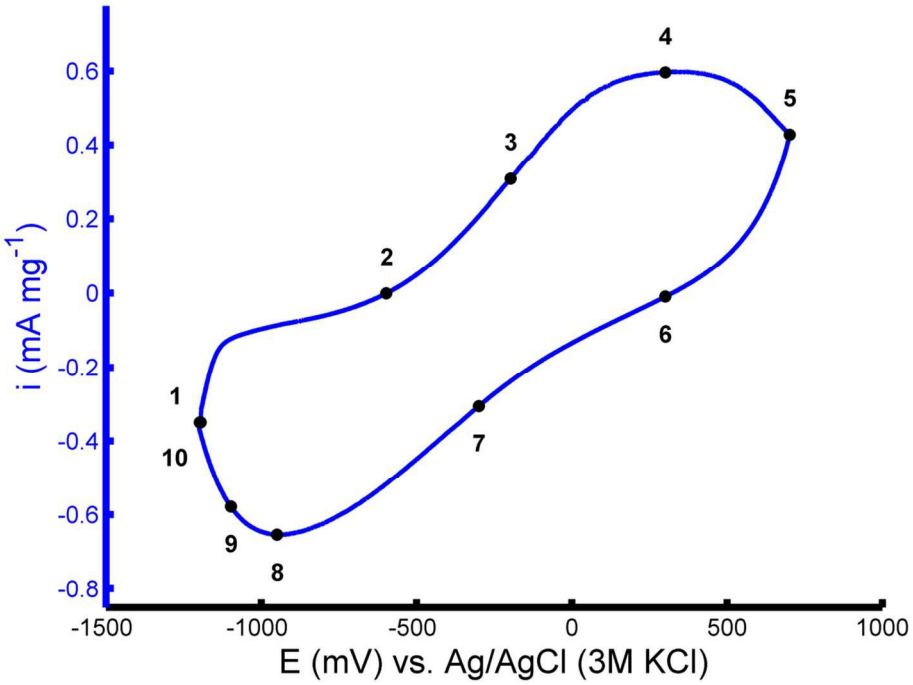

Figure 3 Voltammetric response of PPy-DBS-MWCNT/tape bilayer artificial muscles at 6 mVs^{-1} in the potential range (-1200, 700) mV in 0.1 M NaClO4 aqueous solution with reference points 1 to 10
109x80mm (300 x 300 DPI)

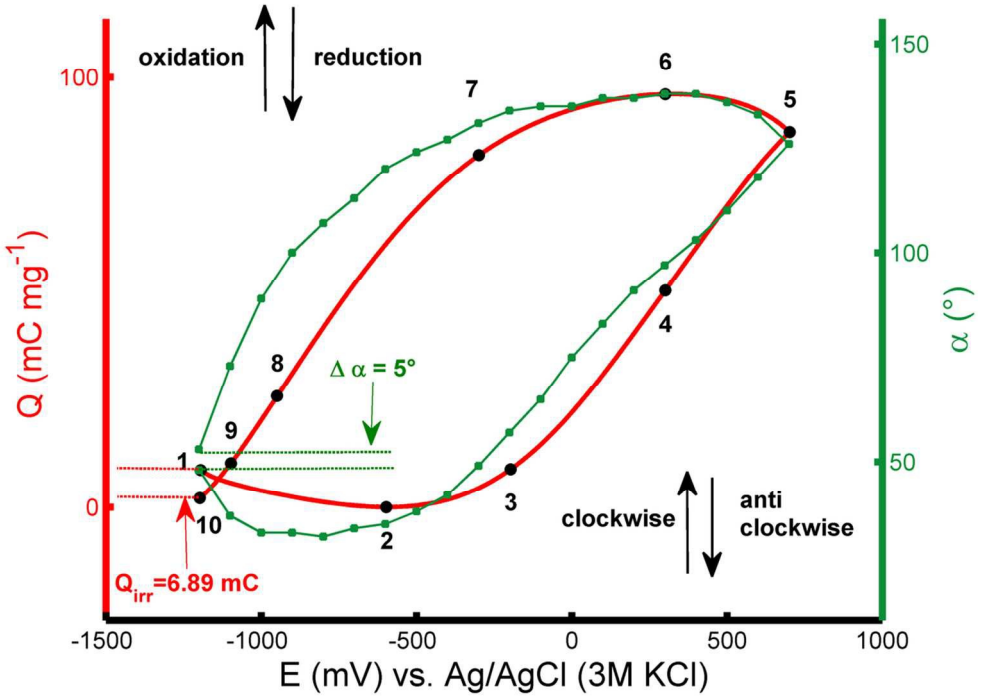

Figure 4 Coulovoltammetric (charge-potential, Q-E, red) with irreversible charge Qirr and dynamo-voltammetric (angle-potential, α-E, green) responses with clockwise angular shift Δα with reference points 1 to 10
109x80mm (300 x 300 DPI)

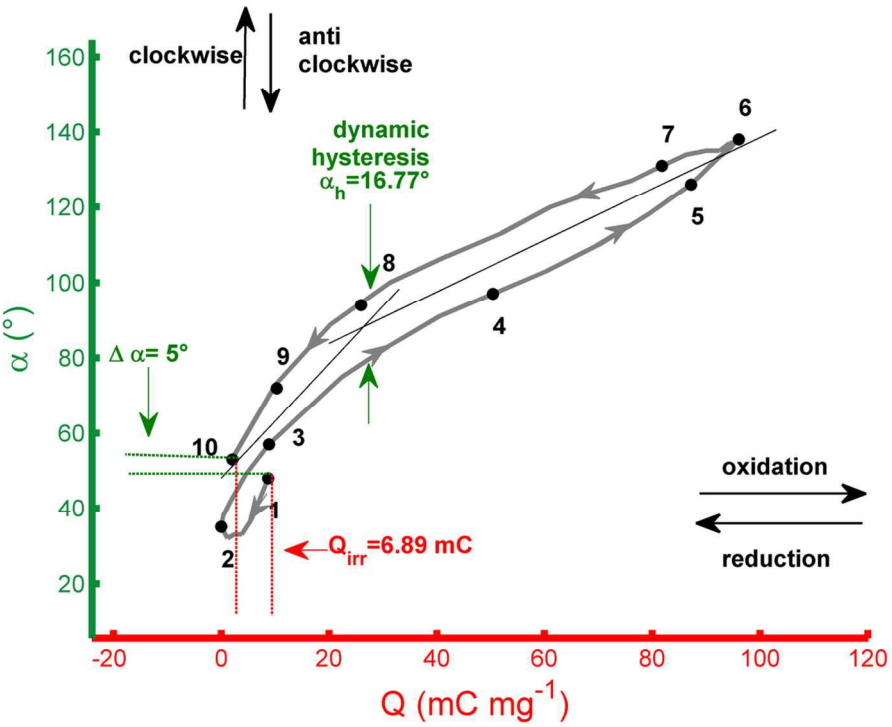

Figure 5 Coulodynamic (angle-charge, α-Q) response with irreversible charge Q_{irr}, angular shift Δα and dynamic hysteresis α_h with reference points 1 to 10
109x80mm (300 x 300 DPI)

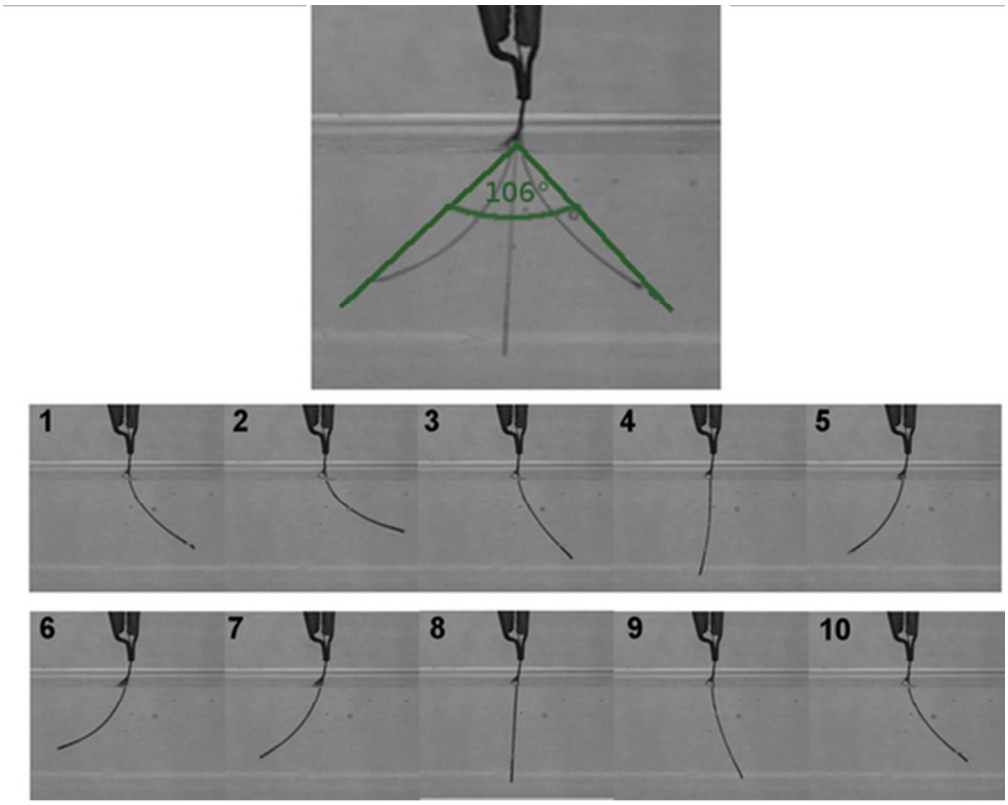

Figure 6 Pictures of the corresponding bending positions at the reference points 1 to 10
45x35mm (300 x 300 DPI)

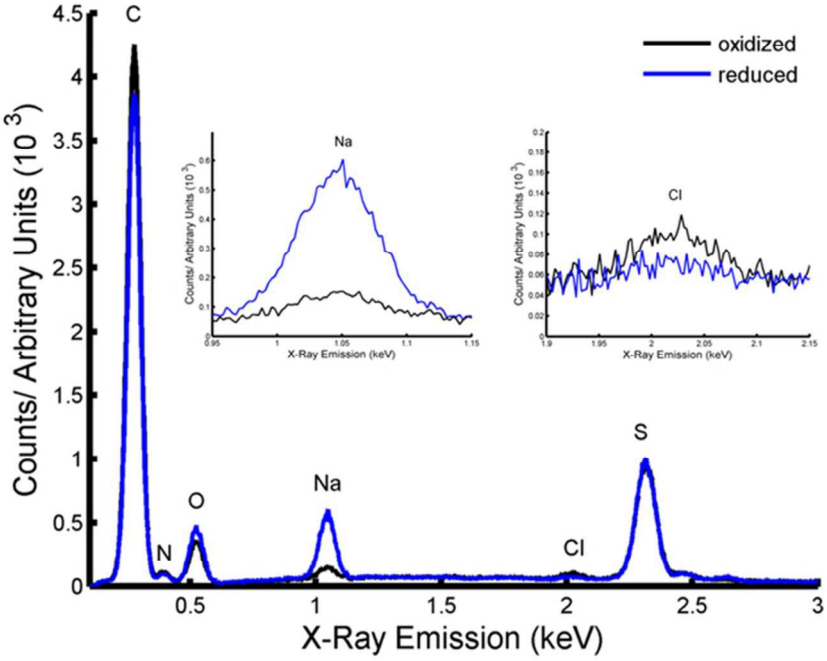

Figure 7 EDX spectra of the PPy-DBS-MWCNT surface at its oxidized (black line) and reduced (blue line) state. Insets show the Na and Cl peaks.
64x46mm (300 x 300 DPI)

Table of Content Entry

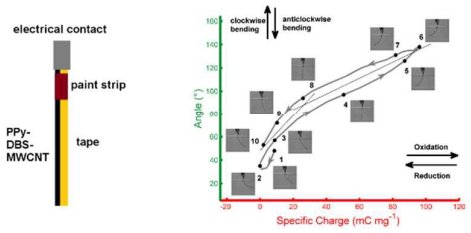

A bilayer full polymeric artificial muscles comprised of electrogenerated PPy-DBS-MWCNT composite and tape was constructed and electrochemical and electrodynamical characterized.